Mathematical Models and Methods in Applied Sciences

AN EFFICIENT NUMERICAL METHOD FOR CAVITATION IN NONLINEAR ELASTICITY

XIANMIN XU*

Institute of Computational Mathematics and Scientific/Engineering Computing, Chinese Academy of Sciences, Beijing 100190, China.
xmxu@lsec.cc.ac.cn

DUVAN HENAO

Laboratoire Jacques-Louis Lions, UMR 7598, CNRS - Univ. Pierre et Marie Curie, Boîte courrier 187, 75252 Paris Cedex 05, France.
henao@ann.jussieu.fr

Received (28 April 2010)
Revised (20 October 2010)
Communicated by (xxxxxxxxxx)

This paper is concerned with the numerical computation of cavitation in nonlinear elasticity. The Crouzeix-Raviart nonconforming finite element method is shown to prevent the degeneration of the mesh provoked by the conventional finite element approximation of this problem. Upon the addition of a suitable stabilizing term to the elastic energy, the method is used to solve cavitation problems in both radially symmetric and non-radially symmetric settings. While the radially symmetric examples serve to illustrate the efficiency of the method, and for validation purposes, the experiments with non-centred and multiple cavities (carried out for the first time) yield novel observations of situations potentially leading to void coalescence.

Keywords: Cavitation; nonconforming FEMs; gradient flow.

AMS Subject Classification 2000: 65N30,74B20,74S05

1. Introduction

Motivated by the study of the internal rupture of rubber cylinders of Gent and Lindley,[13] a number of researchers in nonlinear elasticity have considered the problem of modelling the formation and rapid expansion of voids in solids subjected to tension, phenomenon referred to in the literature as *cavitation*. In the mathematical theory that has developed, hole-creating deformations are obtained as singular minimizers of the stored energy of the material, whenever sufficiently large tensile loads are applied to the body (see, e.g., the seminal work by Ball,[4] the review paper by

*Corresponding author.

Horgan and Polignone,[20] or the more recent works by Müller and Spector,[28] Sivaloganathan and Spector,[36] Conti and De Lellis,[10] and Henao and Mora-Corral[16,17,18]).

Many difficulties arise in the numerical computation of cavitation, especially because the corresponding minimization problems exhibit the Lavrentiev phenomenon,[22] making the traditional finite element methods unable to detect the singular minimizers of the stored energy. Although several methods have been proposed to overcome the Lavrentiev phenomenon,[2,6,21,23,32] they have not been used for the simulation of cavitation (except for the radially symmetric case, see Ref. 21). This is due not only to the nonconvexity and high nonlinearity of the energy functional, but also to the large deformations involved (near the cavity surfaces) and the presence of point singularities.

In order to overcome the mentioned numerical difficulties, we do not consider the full minimization problem, in which all forms of cavitation are allowed to compete in the minimization of the energy, but the simpler situation of the model of Sivaloganathan and Spector (see Ref. 36, 37, 38, 40, 41, among others), where a bound is imposed on the number of cavities, and the possible locations of the singularities in the reference configuration are prescribed. By the approximation result of Sivaloganathan, Spector and Tilakraj[39] (see also Ref. 15), we obtain the singular minimizers for this problem, in the limit as $\epsilon \to 0$, by minimizing the elastic energy, in a class of regular deformations, on a domain with holes of radius ϵ centred at the prescribed cavity points.

For the case of a single cavity at the centre of a ball, Negrón-Marrero and Betancourt[29] were able to carry out computations for the model described above, allowing for non-radially symmetric deformations, by using a spectral-collocation method. For more complex cavitation configurations, however, the efficiency of the traditional numerical methods is affected by the inability to accurately resolve the singularities of the deformation, and by the propensity of these methods to induce the degeneration of the mesh. The purpose of this paper is to show that the singular minimizers arising in the cavitation models can be numerically obtained by using instead the Crouzeix-Raviart nonconforming finite element method,[11] as previously suggested by Ball[7] (for further computations of cavitation in domains with multiple holes, based on a quadratic iso-parametric finite element method, see also the recently completed works by Lian and Li[24,25]).

The structure of this paper is as follows. In Section 2, we briefly introduce the original and regularized energy models. In Section 3, we discuss the finite element approximation of the regularized model. Both the mesh degeneracy of the conforming finite element method, and the lack of this degeneracy in the nonconforming method, are carefully analyzed by means of a scaling argument. Following this analysis, we show that the nonconforming method is prone to its own numerical instability, but that this can be controlled by adding a suitable stabilizing term to the elastic energy. In Section 4, we introduce the corresponding numerical algorithm for the stabilized problem, where minimizers are sought by means of a suitably chosen

gradient flow. In Section 5, we present some radially-symmetric numerical experiments, in order to illustrate the efficiency and the correctness of our method, and present some new observations of cavitation obtained, for the first time, in off-centre configurations and in domains containing multiple cavities.

2. The Energy Model for Cavitation in Nonlinear Elasticity

2.1. *General notation*

We suppose that a nonlinearly elastic body occupies the domain $\Omega \subset \mathbb{R}^n$, $n = 2, 3$, in its reference configuration. Deformations of the body are represented by maps $\mathbf{u} : \Omega \mapsto \mathbb{R}^n$, where $\mathbf{u}(\mathbf{x})$ denotes, for each $\mathbf{x} \in \Omega$, the position of $\mathbf{x}$ in the deformed configuration. The map $\mathbf{u}$ is assumed to be weakly differentiable, and its gradient is denoted by $\nabla \mathbf{u}(\mathbf{x})$.

Vector-valued and matrix-valued quantities are written in boldface. The identity matrix is denoted by $\mathbf{1}$. Given a square matrix $\mathbf{F} \in \mathbb{R}^{n\times n}$, its transpose is denoted by $\mathbf{F}^T$, and its determinant by $\det \mathbf{F}$. The cofactor matrix of $\mathbf{F}$, denoted $\operatorname{cof} \mathbf{F}$, is the matrix satisfying $\mathbf{F}^T \operatorname{cof} \mathbf{F} = (\det \mathbf{F})\mathbf{1}$. The dot product of two vectors $\mathbf{a}, \mathbf{b} \in \mathbb{R}^n$ is denoted by $\mathbf{a} \cdot \mathbf{b}$, and the same notation is used for the inner product of matrices.

2.2. *The model without pre-existing microcavities*

The elastic stored energy of the body is given by

$$I(\mathbf{u}) = \int_\Omega W(\nabla \mathbf{u}) d\mathbf{x}, \tag{2.1}$$

where W is the energy density function. Model examples include the compressible neo-Hookean materials, given by

$$W(\mathbf{F}) = \frac{\mu}{2}(|\mathbf{F}|^2 - 2 \ln \det \mathbf{F} - 3) \tag{2.2}$$

($\mu > 0$ being the shear modulus), or energy densities of the form

$$W(\mathbf{F}) = \frac{\mu}{p}|\mathbf{F}|^p + f(\det \mathbf{F}), \tag{2.3}$$

where $p > 1$ and $f : (0, +\infty) \to R$ is a suitable convex function. The role of f, in general, is to prevent the compression of a subpart of the body to zero volume, or to penalize deviations from incompressibility. For this type of energy densities, certain conditions are required for cavitation to take place[4,28]. We suppose that $n - 1 < p < n$, and that

$$\lim_{s\to 0^+} f(s) = \lim_{s\to+\infty} \frac{f(s)}{s} = +\infty. \tag{2.4}$$

In order to guarantee the existence of minimizers of the energy, deformations are assumed to belong to the Sobolev space $(W^{1,p}(\Omega))^n$, and to satisfy certain invertibility conditions, such as condition (INV) by Müller and Spector,[28] or condition

(INV′) in Ref. 15. For simplicity, we do not give the details of these conditions, but refer to the cited articles.

In this paper we consider the model of Sivaloganathan and Spector,[36] where cavitation is allowed only at a finite number $M \in \mathbb{N}$ of prescribed locations $\mathbf{x}_1, \ldots, \mathbf{x}_M$. This is achieved by imposing that

$$\mathrm{Det}\nabla\mathbf{u} = (\det\nabla\mathbf{u})\mathcal{L}^n + \sum_{i=1}^{M} \alpha_i \delta_{\mathbf{x}_i}, \tag{2.5}$$

where $\mathcal{L}^n$ is the n-dimensional Lebesgue measure, $\delta_{\mathbf{x}_i}$ is the Dirac measure supported on $\mathbf{x}_i$, and the $\alpha_i \geq 0$ are the volumes of the cavities. Here $\mathrm{Det}\nabla\mathbf{u}$ denotes the *distributional determinant* of $\mathbf{u}$ (see Ref. 3, 27), which is defined as

$$\mathrm{Det}\nabla\mathbf{u}(\phi) := -\frac{1}{n}\int_\Omega \mathbf{u}\cdot(\mathrm{cof}\nabla\mathbf{u})\nabla\phi d\mathbf{x}, \qquad \phi \in C_0^\infty(\Omega). \tag{2.6}$$

Upon specifying appropriate boundary conditions, such as $\mathbf{u} = \mathbf{g}$ on $\partial\Omega$ for suitable $\mathbf{g} : \partial\Omega \to \mathbb{R}^n$, the model can be formulated as

$$\min_{\mathbf{u}\in V} I(\mathbf{u}), \tag{2.7}$$

where

$$V = \{\mathbf{u} \in (W^{1,p}(\Omega))^n | \det\nabla\mathbf{u} > 0, \mathbf{u} \text{ satisfies (INV)}, \mathbf{u}|_{\partial\Omega} = \mathbf{g}, \\ \mathrm{Det}\nabla\mathbf{u} = (\det\nabla\mathbf{u})\mathcal{L}^n + \sum_{i=1}^{M} \alpha_i\delta_{\mathbf{x}_i}\}. \tag{2.8}$$

2.3. *The energy model with pre-existing microcavities*

The minimization problem (2.7) exhibits the Lavrientiev phenomenon, whereby

$$\min_{\mathbf{u}\in V\cap(W^{1,\infty})^n} I(\mathbf{u}) > \min_{\mathbf{u}\in V} I(\mathbf{u}),$$

despite the fact that $V\cap(W^{1,\infty})^n$ is dense in V. Because of this, the traditional finite element method fails to give the minimizers and the minimum value of the energy for this problem. In order to overcome this difficulty, we consider the regularized model of Sivaloganathan, Spector and Tilakraj,[39] where small holes of radius ϵ centred at the cavity points are removed from the domain. Letting $\Omega_\epsilon := \Omega\setminus\sum_{i=1}^{M} B(\mathbf{x}_i, \epsilon)$, this can be written as

$$\min_{\mathbf{u}\in V_\epsilon} I_\epsilon(\mathbf{u}), \tag{2.9}$$

where I_ϵ and V_ϵ are given by

$$I_\epsilon(\mathbf{u}) = \int_{\Omega_\epsilon} W(\nabla\mathbf{u})d\mathbf{x}, \tag{2.10}$$

$$V_\epsilon = \{\mathbf{u} \in (W^{1,p}(\Omega_\epsilon))^n | \det\nabla\mathbf{u} > 0, \mathbf{u} \text{ satisfies (INV)}, \mathbf{u}|_{\partial\Omega} = \mathbf{g}, \\ \mathrm{Det}\nabla\mathbf{u} = (\det\nabla\mathbf{u})\mathcal{L}^n\}. \tag{2.11}$$

As shown in Ref. 39 and Ref. 15, the problem (2.9) converges to (2.7) in the sense of Γ-convergence.

3. Finite Element Approximations of the Relaxed Problem

The purpose of this section is to describe some obstacles encountered in a preliminary attempt to carry out computations for (2.9) using the conforming finite element method, and to explain how they were overcome by following instead the Crouzeix-Raviart[11] nonconforming approach.

3.1. *The finite element methods*

Let $\mathcal{T}_h^\epsilon$ be the triangulation of Ω_ϵ. We suppose that all the triangles satisfy the maximum angle principle[1]. We can approximate Ω_ϵ with a polygonal domain, since this introduces only a higher order error. We suppose, thus, that Ω_ϵ is a polygonal domain such that $\Omega_\epsilon = \cup_{K\in\mathcal{T}_h^\epsilon} K$. Define the linear conforming finite element space V_h^c

$$\begin{aligned} V_h^c = \big\{ \mathbf{v} : \mathbf{v}|_K \in (P^1(K))^n, \det\nabla\mathbf{v}|_K > 0, \forall K \in \mathcal{T}_h^\epsilon, \\ \mathbf{v} \in (C(\Omega_\epsilon))^n, \mathbf{v}(\mathbf{a}_i) = \mathbf{g}(\mathbf{a}_i), \forall \mathbf{a}_i \in \partial\Omega \big\}, \end{aligned} \tag{3.1}$$

and the Crouzeix-Raviart nonconforming finite element space

$$\begin{aligned} V_h^{nc} = \big\{ \mathbf{v} : \mathbf{v}|_K \in (P^1(K))^n, \det\nabla\mathbf{v}|_K > 0, \forall K \in \mathcal{T}_h^\epsilon, \\ \mathbf{v} \text{ is continuous on } \mathcal{M}, \mathbf{v}(\mathbf{a}_{ij}) = \mathbf{g}(\mathbf{a}_{ij}), \forall \mathbf{a}_{ij} \in \mathcal{M} \cap \partial\Omega \big\}, \end{aligned} \tag{3.2}$$

where $\mathcal{M}$ denotes the set of mid-points of the edges in $\mathcal{T}_h^\epsilon$.

The conforming and nonconforming finite element approximations of (2.9) are defined, respectively, as

$$\min_{\mathbf{u}_h\in V_h^c} I_h^\epsilon(\mathbf{u}_h), \tag{3.3}$$

and

$$\min_{\mathbf{u}_h\in V_h^{nc}} I_h^\epsilon(\mathbf{u}_h). \tag{3.4}$$

Here $I_h^\epsilon(\mathbf{u}_h)$ is the discrete energy functional

$$I_h^\epsilon(\mathbf{u}_h) = \sum_{K\in\mathcal{T}_h^\epsilon} |K|\ W(\nabla\mathbf{u}_h|_K). \tag{3.5}$$

3.2. *Mesh degeneracy of the conforming finite element method*

By means of a scaling argument, we show how the efficiency of the conforming method is affected by its propensity to make the discrete energy unbounded, and to result in a certain form of mesh degeneracy. For simplicity, consider a domain with a single cavity at the center, $\Omega_\epsilon = \Omega \setminus B(\mathbf{0}, \epsilon)$, and a triangulation $\mathcal{T}_h^\epsilon$ of the

domain, where the inner boundary is approximated by N line segments. For $r > 0$ and $i \in \mathbb{N}$, denote the point with polar coordinates $(r, \frac{\pi i}{N})$ by $A_{r,i}$. We assume that $\partial B(\mathbf{0}, \epsilon)$ is approximated by the segments $\overline{A_{\epsilon,i-2}A_{\epsilon,i}}$, $i = 2, 4, \ldots, 2N$. Furthermore, suppose that the first layer next to the cavity surface is composed of the following two sets of triangles (see Fig. 1):

- those with vertices at $A_{\epsilon,i-1}$, $A_{\epsilon+\delta,i}$ and $A_{\epsilon,i+1}$, for $i = 1, 3, \ldots, 2N-1$; and
- those with vertices at $A_{\epsilon+\delta,i-1}$, $A_{\epsilon,i}$ and $A_{\epsilon+\delta,i+1}$, for $i = 2, 4, \ldots, 2N$.

In both cases, the triangles are denoted K_i, $i = 1, 2, \ldots, 2N$; the height of the triangles is proportional to the parameter $\delta > 0$.

Fig. 1. Vertices $A_{r,i}$ in a triangulation of a domain with microcavities.

When using the conforming element method, great care is needed in choosing N sufficiently large so that the polygon formed by the nodes on the cavity surface accurately resolves the curvature of that surface not only in the reference, but also in the deformed configuration. As schematically described in Fig. 2 and Fig. 3, some of the elements in the first layer may reverse their orientation during the expansion of a microcavity. Fig. 2 shows the polygon $A_{\epsilon,0}A_{\epsilon,2}\cdots A_{\epsilon,2N}$, the circle $\partial B(\mathbf{0}, \epsilon+\delta)$, and the base of an element K_i, with i even. The figure in the middle corresponds to a uniform dilation, while the figure on the right shows a further compression in the radial direction. Fig. 3 represents the same situation, but focuses on the elements themselves. The reason for this degeneracy is that the distance from a curved surface to the mid-point of a line segment with its ends on the same surface will be considerably large compared to the height of the deformed elements (unless the distance between the two end-points is small enough). The remedy is to use very fine meshes, which affects the efficiency of the method. In the calculations that follow, we study the P^1-interpolation of a radially symmetric incompressible deformation, and conclude that δ and N^{-1} should both go to zero, when $\epsilon \to 0$, at least as ϵ^{p-1}.

Fig. 2. Orientation reversal of elements under the conforming approximation.

Fig. 3. Initial and final state of elements at the cavity surface, corresponding to Fig. 2.

Let $\mathbf{u} : \Omega_\epsilon \to \mathbb{R}^2$ be a radially symmetric and incompressible deformation opening a cavity of radius $c > 0$. Writing $\mathbf{u}(\mathbf{x}) = u(|\mathbf{x}|)\frac{\mathbf{x}}{|\mathbf{x}|}$, where u is of class C^1, the

incompressibility condition reads $u'(s)u(s) = s$. Thus,

$$\mathbf{u}(\mathbf{x}) = \sqrt{|\mathbf{x}|^2 + c^2}\,\frac{\mathbf{x}}{|\mathbf{x}|}. \tag{3.6}$$

Suppose now that $\mathbf{u}$ is approximated by its interpolation in V_h^c, given by

$$\mathbf{u}_h|_K = \sum_{i=1}^{3} \mathbf{u}(\mathbf{a}_{i,K})\phi_{i,K}, \qquad\qquad \forall K \in \mathcal{T}_h^\epsilon,$$

where $\mathbf{a}_{i,K}, i = 1, 2, 3$, are coordinates of the nodes of K, and the functions $\phi_{i,K} \in P^1$, which are such that $\phi_{i,K}(\mathbf{a}_{j,K}) = \delta_{ij}$, are the order-one finite element base functions on the triangle K.

Assume the stored-energy function W is of the form (2.3). By considering the elements in the first layer, we observe that

$$I_h^\epsilon(\mathbf{u}_h) \geq \sum_{l=1}^{N} |K_{2l-1}| W(\nabla \mathbf{u}_h|_{K_{2l-1}}) \geq \frac{\mu}{p} \sum_{l=1}^{N} |K_{2l-1}| \big|(\nabla \mathbf{u}_h|_{K_{2l-1}})\big|^p$$

$$\geq \frac{\mu}{p} \sum_{l=1}^{N} |K_{2l-1}| \Big|\nabla \mathbf{u}_h \frac{\mathbf{a}_{2l} - \mathbf{a}_{2l-2}}{|\mathbf{a}_{2l} - \mathbf{a}_{2l-2}|}\Big|^p = \frac{\mu}{p} \sum_{l=1}^{N} |K_{2l-1}| \Big|\frac{\mathbf{u}_h(\mathbf{a}_{2l}) - \mathbf{u}_h(\mathbf{a}_{2l-2})}{|\mathbf{a}_{2l} - \mathbf{a}_{2l-2}|}\Big|^p.$$

Here $\mathbf{a}_i$ denotes the position vector of $A_{\epsilon,i}$, for $i = 0, 2, \ldots, 2N$. A straightforward computation shows that

$$|K_{2l-1}| = \epsilon \sin\frac{\pi}{N}(\delta + 2\epsilon \sin^2\frac{\pi}{2N}), \qquad l = 1, 2, \ldots, N;$$
$$\Big|\frac{\mathbf{u}_h(\mathbf{a}_{2l}) - \mathbf{u}_h(\mathbf{a}_{2l-2})}{|\mathbf{a}_{2l} - \mathbf{a}_{2l-2}|}\Big| = \frac{u(\epsilon)}{\epsilon} \geq \frac{c}{\epsilon}, \qquad l = 1, 2, \ldots, N.$$

For $N \geq 2$ we have that $\sin\frac{\pi}{N} \geq \frac{\pi}{2N}$, hence $I_h^\epsilon(\mathbf{u}_h) \geq \frac{\pi\mu}{2p} c^p \delta \epsilon^{1-p}$. We conclude that, in order for the energy in the first layer to remain bounded, the choice of δ as a function of ϵ must be such that $\delta = O(\epsilon^{p-1})$.

Consider now the potential degeneration of the elements on the cavity surface. The image of K_i, $i = 2, 4, \ldots, 2N$, under the deformation $\mathbf{u}_h$, is the triangle with vertices at

$$(u(\epsilon+\delta), (i-1)\tfrac{\pi}{N}), \quad (u(\epsilon), i\tfrac{\pi}{N}), \quad \text{and} \quad (u(\epsilon+\delta), (i+1)\tfrac{\pi}{N}).$$

Although $u(\epsilon+\delta) > u(\epsilon)$, it is possible for the deformed triangle $\mathbf{u}_h(K_i)$ to become increasingly flat, or even to reverse its orientation (as in Fig. 3), if $N(\epsilon) \not\to \infty$. Indeed, suppose $N^2 < 2c^2/\delta(2\epsilon+\delta)$, then

$$\frac{\delta(2\epsilon+\delta)}{2c} < \frac{\pi^2}{8} N^{-2} \sqrt{(\epsilon+\delta)^2 + c^2}$$

$$\Rightarrow \quad \sqrt{(\epsilon+\delta)^2 + c^2} - \sqrt{\epsilon^2 + c^2} < 2\sqrt{(\epsilon+\delta)^2 + c^2} \sin^2\frac{\pi}{2N}$$

$$\Rightarrow \quad u(\epsilon+\delta)\cos\frac{\pi}{N} < u(\epsilon).$$

Hence N must be larger than $\sqrt{2}c/\sqrt{\delta(2\epsilon+\delta)}$. Since $\delta = O(\epsilon^{p-1})$ and $p < 2$, we obtain $N^{-1} = O(\epsilon^{p-1})$. Hence the conforming method requires the mesh to become extremely fine, both in terms of the height of the triangles and of the number of elements at the cavity surface.

3.3. *Scaling analysis for the Crouzeix-Raviart finite element method*

Denote by $\mathbf{u}$ the radial incompressible deformation (3.6), and let $\tilde{\mathbf{u}}_h$ be its interpolation in the nonconforming finite element space V_h^{nc}. If, given an element $K \in \mathcal{T}_h^\epsilon$, we call $\mathbf{p}_{i,K}$, $i = 1, 2, 3$ the mid-points of its sides, and if we denote the order-one nonconforming finite element base functions on K by $\varphi_{i,K}$, $i = 1, 2, 3$ (so that $\varphi_{i,K}(\mathbf{p}_{j,K}) = \delta_{ij}$), then $\tilde{\mathbf{u}}_h$ is given by

$$\tilde{\mathbf{u}}_h|_K = \sum_{i=1}^{3} \mathbf{u}(\mathbf{p}_{i,K})\varphi_{i,K} \qquad \forall K \in \mathcal{T}_h^\epsilon. \tag{3.7}$$

Suppose that the triangulation in the layer next to the cavity surface is as in the previous subsection. Denote the mid-points of the sides of the elements $K_1, \dots, K_{2N}$ by $\mathbf{p}_1, \dots, \mathbf{p}_{4N+1}$, with $\mathbf{p}_1 = \mathbf{p}_{4N+1}$, as depicted in Fig. 4. More precisely, if we let

$$r_0 = \sqrt{\left(\frac{\epsilon}{2}\cos\frac{\pi}{N} + \frac{\epsilon+\delta}{2}\right)^2 + \left(\frac{\epsilon}{2}\sin\frac{\pi}{N}\right)^2}, \qquad \theta_0 = \arctan\frac{\epsilon\sin\frac{\pi}{N}}{\epsilon\cos\frac{\pi}{N} + \delta + \epsilon}, \tag{3.8}$$

then the mid-points $\mathbf{p}_{2i-1}$, $\mathbf{p}_{2i}$, $\mathbf{p}_{2i+1}$ of the sides of K_i have polar coordinates

$$\begin{aligned} &(r_0, \tfrac{i\pi}{N} - \theta_0), \quad (\epsilon\cos\tfrac{\pi}{N}, \tfrac{i\pi}{N}), \quad (r_0, \tfrac{i\pi}{N} + \theta_0) \qquad i = 1, 3, \dots, 2N-1, \\ &(r_0, \tfrac{(i-1)\pi}{N} + \theta_0), ((\epsilon+\delta)\cos\tfrac{\pi}{N}, \tfrac{i\pi}{N}), (r_0, \tfrac{(i+1)\pi}{N} - \theta_0) \qquad i = 2, 4, \dots, 2N. \end{aligned}$$

Fig. 4. Mid-points of the edges in a triangulation of a domain with microcavities.

The main reasons for the choice of the nonconforming method are that the triangles K_i do not degenerate or reverse their orientation under $\tilde{\mathbf{u}}_h$, and that the energy of $\tilde{\mathbf{u}}_h$ remains close to that of $\mathbf{u}$ (as opposed to the energy of $\mathbf{u}_h$), even if N and δ are kept fixed as $\epsilon \to 0$. Regarding the mesh degeneracy, the most important feature of the method is that by imposing continuity only at the mid-points, and not on the edges in their entirety, it gives each element on the cavity surface the liberty to retain its true orientation, the one dictated by the expansion of the cavity and by the minimization problem. This, which is illustrated in Fig. 5 and Fig. 6[a],

[a]The elements in Fig. 6 ressemble lines in the deformed configuration due to the radial compression (of the order of 10^{-2}). It is observed numerically that the discrete solution is orientation preserving (the determinant is approximately 1.466 in all of the elements, see Section 3.5). Also, we note that the angle made by the base of each element with respect to the curved cavity surface in the deformed configuration is close to the angle made in the reference configuration.

contrasts with the situation in the conforming method, where the orientation of the triangles K_i, with i odd, was forced upon those with i even[b]. Regarding the contribution to the energy of the elements next to the cavity, the main virtue of the method is that the tangential stretch, which constitutes the largest component of the deformation gradient, is given by the stretch of the segment joining the midpoints of the elements. Because of this, it is always of order $c/(\epsilon + \frac{\delta}{2})$, where c is the cavity radius, and so remains bounded as $\epsilon \to 0$, even for constant δ and N. These assertions will be justified and clarified in the subsequent analysis.

Fig. 5. Effect of the conforming and nonconforming finite element methods on the orientation of elements on the cavity surface.

Fig. 6. Elements in the computations of Section 5, initial and final states ($\epsilon = 0.01$, $\delta \approx 0.025$, $N = 15$, $\lambda = 1.8$).

In order to analize the asymptotic behaviour of the relevant quantities for small values of ϵ, and since N and δ will be treated as constants, it is important to precise in what sense certain terms (such as δ^4 or $\delta^2 N^{-2}$) can be considered of higher order, or comparatively smaller, with respect to the main terms in the asymptotic expansions. Before proceeding further, therefore, we specify that expressions of the form

$$f(\epsilon, \delta, N) = g(\epsilon, \delta, N) + O(h(\epsilon, \delta, N))$$

(such as $u(r_0) = c + \frac{1}{2c}(\epsilon + \delta/2)^2 + O\big((\epsilon+\delta)^4\big)$, or $r_0 = \epsilon + \delta/2 + O\big(\epsilon N^{-2}\big)$) will be given the following meaning: for some $\delta_0 > 0$ and $N_0 \in \mathbb{N}$ there exists, for every $\delta < \delta_0$ and every $N > N_0$, constants $\epsilon_0(\delta, N) > 0$ and $C = C(\delta_0, N_0) > 0$ such that

$$\epsilon < \epsilon_0(\delta, N) \quad \Rightarrow \quad |f(\epsilon, \delta, N) - g(\epsilon, \delta, N)| < Ch(\epsilon, \delta, N).$$

We study first the behaviour of $\nabla \tilde{\mathbf{u}}_h^{(N)}|_{K_i}$ for i even. Writting

$$\mathbf{e}_1 := (\cos\frac{i\pi}{N}, \sin\frac{i\pi}{N}), \quad \mathbf{e}_2 := (-\sin\frac{i\pi}{N}, \cos\frac{i\pi}{N}), \quad \tilde{\mathbf{p}} = \frac{\mathbf{p}_{2i-1} + \mathbf{p}_{2i+1}}{2} \tag{3.9}$$

we have that

$$(\nabla \tilde{\mathbf{u}}_h|_{K_i})\mathbf{e}_1 = \frac{\mathbf{u}(\mathbf{p}_{2i}) - \mathbf{u}(\tilde{\mathbf{p}})}{|\mathbf{p}_{2i} - \tilde{\mathbf{p}}|} = \frac{u\big((\epsilon+\delta)\cos\frac{\pi}{N}\big) - u(r_0)\cos(\frac{\pi}{N} - \theta_0)}{(\epsilon+\delta)\cos\frac{\pi}{N} - r_0\cos(\frac{\pi}{N} - \theta_0)}\,\mathbf{e}_1 \tag{3.10}$$

$$(\nabla \tilde{\mathbf{u}}_h|_{K_i})\mathbf{e}_2 = \frac{\mathbf{u}(\mathbf{p}_{2i+1}) - \mathbf{u}(\mathbf{p}_{2i-1})}{|\mathbf{p}_{2i+1} - \mathbf{p}_{2i+1}|} = \frac{2u(r_0)\sin(\frac{\pi}{N} - \theta_0)}{2r_0\sin(\frac{\pi}{N} - \theta_0)}\,\mathbf{e}_2 = \frac{u(r_0)}{r_0}\,\mathbf{e}_2\,. \tag{3.11}$$

[b]In the sense that the direction, in the deformed configuration, of the segments $\overline{A_{\epsilon+\delta,i-1}A_{\epsilon,i}}$ and $\overline{A_{\epsilon+\delta,i+1}A_{\epsilon,i}}$, for i even, is determined by the image of $\mathbf{u}_h(K_{i-1})$ and $\mathbf{u}_h(K_{i+1})$.

Let $\mathbf{a}_i, \mathbf{a}_{i-1}$ denote the position vectors of $A_{\epsilon,i}, A_{\epsilon+\delta,i-1}$, respectively. From (3.8) we deduce that

$$r_0 \cos\theta_0 = (\epsilon+\delta/2) - \epsilon \sin^2 \frac{\pi}{2N}, \qquad \sin\theta_0 = \epsilon \sin\frac{\pi}{N}/2r_0, \tag{3.12}$$

$$(\epsilon+\delta)/2 < r_0 = |\mathbf{a}_i + \mathbf{a}_{i-1}|/2 < (|\mathbf{a}_i| + |\mathbf{a}_{i-1}|)/2 = \epsilon + \delta/2. \tag{3.13}$$

Using that $\sin\frac{\pi}{2N} < \frac{\pi}{2N}$ we obtain

$$r_0 = r_0\cos\theta_0 + 2r_0 \sin^2\frac{\theta_0}{2} = (\epsilon+\delta/2) + O(\epsilon N^{-2}). \tag{3.14}$$

This, combined with $|\sqrt{1+t} - (1 + t/2 - t^2/8)| < |t^3/2|$, for $t \in (-1,\infty)$, and with $|t - \sin t| < |t^3/6|$, for all $t \in \mathbb{R}$, yields

$$\frac{\pi}{N} - \theta_0 = \frac{\pi}{N}\left(1 + O\big(\epsilon/(\epsilon+\delta)\big)\right), \quad \frac{1}{r_0} = 2\delta^{-1}(1 + O\big(\epsilon\delta^{-1}\big)) \tag{3.15}$$

$$u(r_0) = c + \frac{1}{2c}(\epsilon+\delta/2)^2 - \frac{1}{8c^3}(\epsilon+\delta/2)^4 + O((\epsilon+\delta)^6). \tag{3.16}$$

From (3.15), (3.16), and (3.11) we find

$$\frac{u(r_0)}{r_0} = 2c\delta^{-1}(1 + \frac{1}{8c^2}\delta^2 + O(\delta^4)). \tag{3.17}$$

Using once again the estimate for $\sqrt{1+t}$, we have that

$$(\epsilon+\delta)\cos\frac{\pi}{N} = (\epsilon+\delta)(1 - 2\sin^2\frac{\pi}{2N}) = (\epsilon+\delta)(1 + O(N^{-2})), \tag{3.18}$$

$$u\big((\epsilon+\delta)\cos\frac{\pi}{N}\big) = c + \frac{1}{2c}\delta^2 - \frac{1}{8c^3}\delta^4 + O(\delta^6) + O(\delta^2 N^{-2}). \tag{3.19}$$

As a consequence of (3.15), we have that $\cos(\frac{\pi}{N} - \theta_0) = 1 + O(N^{-2})$. Hence

$$u(r_0)\cos(\frac{\pi}{N} - \theta_0) = c\big(1 + \frac{1}{8c^2}\delta^2 - \frac{1}{128c^4}\delta^4 + O(\delta^6) + O(N^{-2})\big). \tag{3.20}$$

In order to find $(\nabla\tilde{\mathbf{u}}_h|_{K_i})\mathbf{e}_1$ it only remains to compute $r_0\cos(\frac{\pi}{N} - \theta_0)$, which, by virtue of (3.14), is given by

$$r_0\cos(\frac{\pi}{N} - \theta_0) = (\epsilon+\delta/2)(1 + O(N^{-2})). \tag{3.21}$$

Combining (3.10), (3.19), (3.20), (3.18), and (3.21) we arrive at

$$\Big|(\nabla\tilde{\mathbf{u}}_h|_{K_i})\mathbf{e}_1\Big| = c^{-1}\delta\big(\frac{3}{4} - \frac{15}{64c^2}\delta^2 + O(\delta^4) + O(\delta^{-2}N^{-2})\big). \tag{3.22}$$

For the case of K_i with i odd, defining $\mathbf{e}_1$ and $\mathbf{e}_2$ as in (3.9) we have

$$(\nabla\tilde{\mathbf{u}}_h|_{K_i})\mathbf{e}_1 = \frac{u(r_0)\cos\theta_0 - u(\epsilon\cos\frac{\pi}{N})}{r_0\cos\theta_0 - \epsilon\cos\frac{\pi}{N}}\,\mathbf{e}_1, \qquad (\nabla\tilde{\mathbf{u}}_h|_{K_i})\mathbf{e}_2 = \frac{u(r_0)}{r_0}\,\mathbf{e}_2.$$

Proceeding as before, we obtain $\cos\theta_0 = 1 + O\big(\epsilon^2 N^{-2}/(\epsilon+\delta)^2\big)$,

$$\begin{aligned} u(r_0)\cos\theta_0 - u(\epsilon\cos\frac{\pi}{N}) &= \frac{\delta^2}{4c}\left(1 - \frac{\delta^2}{32c^2} + O(\delta^4)\right) \\ \frac{1}{r_0\cos\theta_0 - \epsilon\cos\frac{\pi}{N}} &= 2\delta^{-1}\left(1 + O\big(\epsilon N^{-2}\delta^{-1}\big)\right) \\ (\nabla\tilde{\mathbf{u}}_h|_{K_i})\mathbf{e}_1 &= \frac{\delta}{4c}\left(1 - \frac{1}{16c^2}\delta^2 + O(\delta^4)\right) \end{aligned} \tag{3.23}$$

In both cases (see (3.22), (3.23)), $(\nabla\tilde{\mathbf{u}}_h|_{K_i})\mathbf{e}_1 = O(\delta)$. From (3.14) and (3.16) we obtain

$$\frac{u(r_0)}{r_0} = \frac{2c}{2\epsilon+\delta}\left(1 + O\big((\epsilon+\delta)^2\big)\right).$$

Hence, for $i = 1, 2, \ldots, 2N$,

$$\begin{aligned} |\nabla\tilde{\mathbf{u}}_h|_{K_i}|^p &= \left|\frac{u(r_0)}{r_0}\right|^p \left(1 + \left|\frac{(\nabla\tilde{\mathbf{u}}_h|_{K_i})\mathbf{e}_1}{u(r_0)/r_0}\right|^2\right)^{p/2} \\ &= \left|\frac{2c}{2\epsilon+\delta}\right|^p \left(1 + O\big((\epsilon+\delta)^2\big)\right)\left(1 + O\big(\delta^2(\epsilon+\delta)\big)\right) \\ &= 2^p c^p (2\epsilon+\delta)^{-p}\left(1 + O\big((\epsilon+\delta)^2\big)\right). \end{aligned} \tag{3.24}$$

This estimate allows us to compare

$$E_1 = \int_{\epsilon<|\mathbf{x}|<\epsilon+\delta} |\nabla\mathbf{u}|^p d\mathbf{x} = \pi\int_{\epsilon^2}^{(\epsilon+\delta)^2}\left(2 + \frac{c^4}{t(t+c^2)}\right)^{\frac{p}{2}} dt$$

against

$$E_{1h} = \sum_{i=1}^{2N} |K_i|\,|\nabla\tilde{\mathbf{u}}_h|_{K_i}|^p = N|K_1|\,|\nabla\tilde{\mathbf{u}}_h|_{K_1}|^p + N|K_2|\,|\nabla\tilde{\mathbf{u}}_h|_{K_2}|^p.$$

Using that $\left(2 + \frac{c^4}{t(t+c^2)}\right)^{\frac{p}{2}} = c^p t^{-\frac{p}{2}} + O(t^{1-\frac{p}{2}})$, we obtain

$$E_1 = \frac{2\pi c^p}{2-p}(\epsilon+\delta)^{2-p}\left(1 - \big(\epsilon/(\epsilon+\delta)\big)^{2-p} + O\big(\delta(\epsilon+\delta)\big)\right).$$

As for E_{1h}, notice that

$$|K_1| = \epsilon\delta\frac{\pi}{N}(1 + O(N^{-2})), \qquad |K_2| = \delta(\epsilon+\delta)\frac{\pi}{N}(1 + O(N^{-2})),$$

hence

$$E_{1h} = 2^p\pi c^p\delta(2\epsilon+\delta)^{1-p}\big(1 + O(N^{-2}) + O((\epsilon+\delta)^2)\big).$$

We conclude that E_1 and E_{1h} are of the same order of magnitude (namely, of order δ^{2-p}), in contrast to the situation in the conforming method, where $E_{1h} \to \infty$ as $\epsilon \to 0$.

3.4. *Instability of the nonconforming finite element method*

Some care is needed when using the Crouzeix-Raviart method, due to its propensity to obtain pathological solutions to the equilibrium equations as the one depicted in Fig. 7. In this figure the elements near $\partial\Omega$ stretch in one direction (because of the boundary condition), but compress in the other (so as to preserve the volume of the elements), creating discontinuities throughout the mesh in its entirety[c]. These solutions are obtained because of the flexibility of the method, where the elements can choose their own orientation independently of the orientation of their neighbouring elements. As explained in the previous subsections, such behaviour is desirable on the cavity surface, but it is inadmissible in the interior and on the outer boundary.

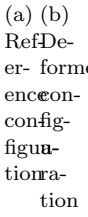

Fig. 7. Instability of the Crouzeix-Raviart finite element method; $\epsilon = 0.01$, stored-energy function Eq. (5.1).

Similar instabilities have been observed for problems in linear elasticity and in fluid dynamics (see, e.g., Ref. 12 and Ref. 9), and are related to the lack of a discrete Korn's inequality in the nonconforming setting. For these problems the Crouzeix-Raviart method is stabilized by penalizing the jump of the discrete function on the sides of all inner elements. However, numerical experiments reveal this to be insufficient in the cavitation problem. Fig. 8 shows a numerical solution to (3.4) using the L^2 penalty term

$$\frac{C}{h}\sum_{E\in\mathcal{E}}\int_E |[\mathbf{u}_h]|^2 ds, \tag{3.25}$$

where C is a constant, h and $\mathcal{E}$ are the size parameter and the set of sides of the triangulation, and $[\,\cdot\,]$ denotes the jump of a given quantity across the corresponding side. Even though the solution is correct near the boundary, the pathological behaviour persists in the interior of the body. This can only be solved by increasing the value of C considerably as the mesh becomes finer.

[c]The instability continues to be observed even for very fine meshes.

Fig. 8. Instability of the Crouzeix-Raviart method using the L^2 penalty term (3.25); $\epsilon = 0.01$, stored-energy function (5.1).

For the nonlinear problem under consideration, we stabilize the Crouzeix-Raviart approximation by adding

$$\frac{C}{h}\sum_{E\in\mathcal{E}}\int_E |[\nabla \mathbf{u}_h \cdot \mathbf{s}]|^2 ds \tag{3.26}$$

to the discrete energy, penalizing the orientation mismatch between neighbouring elements across the sides. Here C, h, $\mathcal{E}$, and $[\,\cdot\,]$ are as in (3.25)[d], and $\mathbf{s}$ denotes one of the two unit vectors in the direction of E (its orientation being suitably specified). With this penalty term the behaviour in Fig. 7 and Fig. 8 becomes expensive because $[\nabla \mathbf{u}_h \cdot \mathbf{s}]$ remains essentially of the same magnitude, independently of the smallness of the elements. Indeed, $|[\nabla \mathbf{u}_h \cdot \mathbf{s}]|$ depends only on the difference in direction, in the deformed configuration, between corresponding sides of adjacent elements (in contrast, e.g., to $|[\mathbf{u}_h]|$, which is proportional to the length of the edges). The price to pay is thus of the order of $h^{-1}\sum_{E\in\mathcal{E}} \ell(E) \sim h^{-1} n_E h \sim h^{-2}$, where we have denoted by $\ell(E)$ the length of E and by n_E the total number of elements.

In our numerical experiments, the penalty term is observed to provide the stability necessary for the method to find the true solutions of the minimization problem, rather than the unexpected local minimizers described previously. Nevertheless, the analysis of the penalization scheme remains an important open problem, both for discontinuous Galerkin methods and for nonconforming finite element methods. In the case of cavitation, we may argue that $|[\nabla \mathbf{u}_h \cdot \mathbf{s}]|$ is of the order of $\delta^{-1}\sin\frac{\pi}{N}$ near the cavity surface, and, hence, that the penalty term for the true solution to the problem (using nonconforming elements) is of the order of

$$h^{-1}(\delta^{-1}N^{-1})^2 N(\delta + N^{-1}) = \frac{N^{-1}}{h\delta}(1 + h\frac{N^{-1}}{h\delta})$$

(the last two factors on the left-hand side corresponding to the number of elements in the first layer, and to their perimeters, respectively). This suggests that the price to pay, in the actual solution, for the orientation mismatch of the elements on the cavity surface (depicted in Fig. 5 and discussed in Section 3.3) is sufficiently small, at least if $N^{-1} \ll h\delta$. Numerically, we observe that the penalty term is indeed small, even in situations where the condition on N, h, and δ is not satisfied, such as the one in Fig. 6 in which $\delta \approx 0.025$ and $N = 15$.

[d]The actual values of C and h in our computations being 0.05 and $n_E^{-1/2}$, respectively, where n_E denotes the total number of elements.

3.5. *Jacobian determinant at the cavity surface*

From the work of Ball[5] (see also Sect. 2.4 in Ref. 8, Thm. 5.1 in Ref. 36), it follows that minimizers of (2.10) satisfy the Eulerian form of the equilibrium equations:

$$\int_\Omega \left[\nabla W\big(\nabla \mathbf{u}(\mathbf{x})\big)\nabla \mathbf{u}(\mathbf{x})^T\right]\cdot \nabla \boldsymbol{\varphi}\big(\mathbf{u}(\mathbf{x})\big)dx = 0,$$

for all $\boldsymbol{\varphi} \in C^1(\mathbb{R}^n, \mathbb{R}^n)$ such that $\boldsymbol{\varphi}$ and $\nabla\boldsymbol{\varphi}$ are uniformly bounded and satisfy $\boldsymbol{\varphi}\circ\mathbf{u}|_{\partial\Omega} = 0$ in the sense of traces. If $\mathbf{u}$ is sufficiently regular in $\overline{\Omega_\epsilon}$, so that $\mathbf{u}(\Omega_\epsilon)$ is open and the cavities have sufficiently regular boundaries, the equilibrum equations imply that $\mathbf{T}(\mathbf{y})\boldsymbol{\nu}(\mathbf{y}) = \mathbf{0}$ at every $\mathbf{y}$ on the surface of any of the cavities, where $\mathbf{T}$ stands for the Cauchy-stress tensor

$$\mathbf{T}(\mathbf{y}) = \nabla W(\nabla \mathbf{u}(\mathbf{x}))\nabla \mathbf{u}(\mathbf{x})^T(\det\nabla \mathbf{u}(\mathbf{x}))^{-1}, \quad \mathbf{y} = \mathbf{u}(\mathbf{x}),$$

and $\boldsymbol{\nu}(\mathbf{y})$ represents the unit normal to the cavity. Taking the dot product with $\boldsymbol{\nu}$, and applying this condition to the energy function (2.3), we obtain

$$f'(\det\nabla \mathbf{u}(\mathbf{x})) = -\mu|\nabla \mathbf{u}(\mathbf{x})|^{p-2}\left|\frac{\nabla \mathbf{u}(\mathbf{x})^T}{\det\nabla \mathbf{u}(\mathbf{x})}\boldsymbol{\nu}(\mathbf{u}(\mathbf{x}))\right|^2 \det\nabla \mathbf{u}(\mathbf{x}),$$

$\mathbf{x} \in \partial B_\epsilon(\mathbf{x}_i)$, $i = 1, \dots, M$. From the convexity of f and the fact that $f(s)$ is increasing for large values of s, it follows that $\det\nabla\mathbf{u} \le s^*$ at the cavity surface, where s^* denotes the minimizer of f. Note that $\frac{\nabla\mathbf{u}^T}{\det\nabla\mathbf{u}} = \operatorname{cof}\nabla\mathbf{u}^{-1}$, and that $|(\operatorname{cof}\nabla\mathbf{u}^{-1}(\mathbf{y}))\boldsymbol{\nu}(\mathbf{y})|$ gives the infinitesimal change in area, due to $\mathbf{u}^{-1}$, at the cavity surface. If the expansion of the cavities is uniform, in the sense that $|(\operatorname{cof}\nabla\mathbf{u}^{-1})\boldsymbol{\nu}|$ is approximately constant on the boundary of the cavity, we obtain that

$$|f'(\det\nabla\mathbf{u})| \le C\left(\frac{c}{\epsilon}\right)^{p-2-2(n-1)},$$

where c denotes the radius of the cavity. From this we observe that $\det\nabla\mathbf{u}$ converges to s^*, as $\epsilon\to 0$, at every point on the cavity surface.[e]

Fig. 9. Jacobian determinant of the numerical solution using the Crouzeix-Raviart finite element method.

The previous is a formal calculation, but numerically it is indeed observed that $\det\nabla\mathbf{u} \approx s^*$ on the cavity surface. For the energy function (5.2), where $f(s) = \frac{1}{2}(s-1)^2 + s^{-1}$, the numerical solution $\mathbf{u}_h$ is such that $\det\nabla\mathbf{u}_h|_{K_i}$ is close to 1.4656 (the minimizer of f) for every $i = 1, \dots, 2N$ (see Fig. 9). This contrasts with the interpolation $\tilde{\mathbf{u}}_h$ of the radial incompressible solution (studied in Section 3.3), where

$$\det\nabla\tilde{\mathbf{u}}_h|_{K_i} = \frac{3}{2} - \frac{9}{32c^2}\delta^2 + O(\delta^4) + O(\delta^{-2}N^{-2}), \quad i = 2, 4, \dots, 2N,$$
$$\det\nabla\tilde{\mathbf{u}}_h|_{K_i} = \frac{1}{2} + \frac{1}{32c^2}\delta^2 + O(\delta^4), \quad i = 1, 3, \dots, 2N-1$$

[e]The argument is based on Sect. 7.5 in Ref. 4; see also Eq. 33 in Ref. 30.

(the expansions are obtained by multiplying (3.22) and (3.17), considering that $\{\mathbf{e}_1, \mathbf{e}_2\}$ is an orthonormal basis). The reason for this discrepancy is that the numerical solution will adjust itself, abandonning the pointwise convergence to the interpolation $\tilde{\mathbf{u}}_h$ at the nodes close to the cavity surface, in order to favour the convergence of the Jacobian determinants. Given the structure of the energy function, and its direct dependence on the determinant, the convergence of this quantity becomes much more relevant for the minimization of the energy.

The validity of the scaling analysis of the previous subsections is not affected by the above discrepancy between $\mathbf{u}_h$ and $\tilde{\mathbf{u}}_h$, since the slight difference between $\mathbf{u}_h(\mathbf{p}_i)$ and $\tilde{\mathbf{u}}_h(\mathbf{p}_i)$, for $i = 1, \dots, 4N$, does not have a great effect on the estimates for the tangential derivatives, which are the most relevant for the study of the contributions to the energy. What is important (as mentioned after Eq. (3.8)), is that the tangential stretch $u(r_0)/r_0$ is computed at the midpoints of the elements, hence it is of order $2c\delta^{-1}$ (c being the cavity radius), and not $c\epsilon^{-1}$. This makes the method efficient in that it does not require excessively fine meshes.

Since $\det \nabla \mathbf{u}_h$ is close to 1.4656 in the elements close to the cavity (as proved numerically), these elements do not become flat or reverse their orientation as under the conforming method. The flexibility expected of the nonconforming method for the orientation of the elements close to the surface (illustrated in Fig. 5), is also corroborated numerically.

We end by noting that the average determinant in the inner layer, $(\frac{3}{2} + \frac{1}{2})/2$, coincides with the determinant of the radial incompressible deformation. Both the oscillating behaviour of $\det \nabla \tilde{\mathbf{u}}_h|_{K_i}$ and the before-mentioned agreement should be taken into account in a rigorous proof of convergence of the nonconforming method for the problem of cavitation, and potentially for other nonconvex variational problems with singular minimizers.

4. The Numerical Method and Gradient Flows

4.1. *The gradient flow equations*

We look for minimizers of (2.9) by solving its corresponding H_0^1 gradient flow

$$\begin{aligned} -\Delta \mathbf{u}_t(\mathbf{x}, t) &= \operatorname{div}(\nabla W(\nabla \mathbf{u}(\mathbf{x}, t))), \quad \mathbf{x} \in \Omega_\epsilon, \quad t > 0, \\ \mathbf{u}(\mathbf{x}, t) &= \mathbf{g}(\mathbf{x}), \quad \mathbf{x} \in \partial\Omega, \quad t > 0, \\ (\nabla \mathbf{u}_t + \nabla W(\nabla \mathbf{u}))\boldsymbol{\nu}(\mathbf{x}) &= \mathbf{0}, \quad \mathbf{x} \in \partial B_\epsilon(\mathbf{x}_i),\ i = 1, \dots, M, \quad t > 0, \end{aligned} \tag{4.1}$$

($\boldsymbol{\nu}(\mathbf{x})$ being the unit normal to $\partial B_\epsilon(\mathbf{x}_i)$) in its weak form given by

$$\int_{\Omega_\epsilon} \nabla \mathbf{u}_t \cdot \nabla \mathbf{v} = -\int_{\Omega_\epsilon} (\mu|\nabla \mathbf{u}|^{p-2}\nabla \mathbf{u} + f'(\det\nabla \mathbf{u})\mathrm{cof}\nabla \mathbf{u}) \cdot \nabla \mathbf{v} dx, \quad \forall \mathbf{v} \in V_0\,, \tag{4.2}$$

with $V_0 := \{\mathbf{v} \in (W^{1,p}(\Omega_\epsilon))^n | \, \mathbf{v} = \mathbf{0} \text{ on } \partial\Omega\}$. Eq. (4.1) gives a steepest descent iteration for minimizing the stored energy functional, as seen from

$$\begin{aligned} \frac{dI(\mathbf{u})}{dt} &= \int_{\Omega_\epsilon} (\mu|\nabla \mathbf{u}|^{p-2}\nabla \mathbf{u} + f'(\det\nabla \mathbf{u})\mathrm{cof}\nabla \mathbf{u}) \cdot \nabla \mathbf{u}_t dx \\ &= -\int_{\Omega_\epsilon} \nabla \mathbf{u}_t \cdot \nabla \mathbf{u}_t dx \le 0, \end{aligned} \tag{4.3}$$

and is known to provide a faster and more stable numerical scheme than, for example, the L^2 gradient flow

$$\mathbf{u}_t = \mathrm{div}(\mu|\nabla \mathbf{u}|^{p-2}\nabla \mathbf{u} + f'(\det\nabla \mathbf{u})\mathrm{cof}\nabla \mathbf{u}) \tag{4.4}$$

(see, e.g., Ch. 2 and Sect. 11.6 in Ref. 31). In their computations of cavitation, Negrón-Marrero and Betancourt[29] have used a Richardson extrapolation technique, based on the equation

$$\mathbf{u}_{tt} + \eta \mathbf{u}_t = \mathrm{div}(\mu|\nabla \mathbf{u}|^{p-2}\nabla \mathbf{u} + f'(\det\nabla \mathbf{u})\mathrm{cof}\nabla \mathbf{u}), \quad \eta \ll 1, \tag{4.5}$$

for which the Courant-Friedrichs-Lewy condition (see, e.g., Ref. 26) is not as restringent as for (4.4). Denoting the time step by δt and the mesh size by h, the CFL condition for (4.5) and for (4.4) reads $\delta t = O(h)$ and $\delta t = O(h^2)$, respectively. Due to the presence of the Laplacian operator in front of $\mathbf{u}_t$, in the case of (4.1) the condition becomes $\delta t = O(1)$. This has motivated the choice of our method, whose efficiency is comprobated in the numerical experiments.

4.2. *The discretization and the numerical algorithm*

To discretize the above equations, we introduce the finite element space

$$\begin{aligned} V_{h,0}^{nc} = \big\{\mathbf{v} : \mathbf{v}|_K \in (P^1(K))^n, \ \mathbf{v} \text{ is continuous on } \mathcal{M}, \\ \mathbf{v}(\mathbf{a}_{ij}) = \mathbf{0} \ \forall \mathbf{a}_{ij} \in \mathcal{M} \cap \partial\Omega\big\}\,. \end{aligned} \tag{4.6}$$

We discretize (4.2) in space using the nonconforming finite element method. Taking into account the stabilization term (3.26), we obtain the semi-discrete equation

$$\begin{aligned} \sum_{K\in\mathcal{T}} \int_K \nabla \frac{\mathrm{d}\mathbf{u}_h}{\mathrm{d}t} \cdot \nabla \mathbf{v}_h = &-\sum_{K\in\mathcal{T}} \int_K (\mu|\nabla \mathbf{u}_h|^{p-2}\nabla \mathbf{u}_h + f'(\det\nabla \mathbf{u}_h)\mathrm{cof}\nabla \mathbf{u}_h) \cdot \nabla \mathbf{v}_h dx \\ &-\frac{C}{h}\sum_{E\in\mathcal{E}} \int_E [\nabla \mathbf{u}_h \cdot \mathbf{s}][\nabla \mathbf{v}_h \cdot \mathbf{s}] ds, \qquad \forall \mathbf{v}_h \in V_{h,0}^{nc}. \end{aligned} \tag{4.7}$$

Let now $0 = t_0 < t_1 < t_2 < \ldots < t_N = T < \infty$, and replace the time derivative at each t_n by the forward difference

$$\frac{\mathrm{d}\mathbf{u}_h}{\mathrm{d}t}|_{t=t_n} \approx \frac{\mathbf{u}_h^{n+1} - \mathbf{u}_h^n}{t_{n+1} - t_n}.$$

For $n = 0, 1, \cdots$ we obtain

$$\begin{aligned}
&\sum_{K\in\mathcal{T}} \int_K \nabla \frac{\mathbf{u}_h^{n+1} - \mathbf{u}_h^n}{t_{n+1} - t_n} \cdot \nabla \mathbf{v}_h \\
&= -\sum_{K\in\mathcal{T}} \int_K (\mu |\nabla \mathbf{u}_h^n|^{p-2} \nabla \mathbf{u}_h^n + f'(\det \nabla \mathbf{u}_h^n) \mathrm{cof} \nabla \mathbf{u}_h^n) \cdot \nabla \mathbf{v}_h dx \\
&\quad - \frac{C}{h} \sum_{E\in\mathcal{E}} \int_E [\nabla \mathbf{u}_h^n \cdot \mathbf{s}][\nabla \mathbf{v}_h^n \cdot \mathbf{s}] ds, \qquad \forall \mathbf{v}_h \in V_{h,0}^{nc}.
\end{aligned} \tag{4.8}$$

In the computations, we set $\mathbf{w}_h = \frac{\mathbf{u}_h^{n+1} - \mathbf{u}_h^n}{t_{n+1} - t_n}$ and solve

$$\begin{aligned}
&\sum_{K\in\mathcal{T}} \int_K \nabla \mathbf{w}_h \cdot \nabla \mathbf{v}_h \\
&= -\sum_{K\in\mathcal{T}} \int_K (\mu |\nabla \mathbf{u}_h^n|^{p-2} \nabla \mathbf{u}_h^n + f'(\det \nabla \mathbf{u}_h^n) \mathrm{cof} \nabla \mathbf{u}_h^n) \cdot \nabla \mathbf{v}_h dx \\
&\quad - \frac{C}{h} \sum_{E\in\mathcal{E}} \int_E [\nabla \mathbf{u}_h^n \cdot \mathbf{s}][\nabla \mathbf{v}_h^n \cdot \mathbf{s}] ds, \qquad \forall \mathbf{v}_h \in V_{h,0}^{nc}.
\end{aligned} \tag{4.9}$$

at each time step. Then we compute $\mathbf{u}_h^{n+1} = \mathbf{u}_h^n + (t_{n+1} - t_n)\mathbf{w}_h$ to find the solution of the next step.

Denoting the set of nodes of the triangulation by $\mathcal{N}$, define the norm $\|\mathbf{w}_h\|$ by $\|\mathbf{w}_h\|^2 := \sum_{\mathbf{a}\in\mathcal{N}} |\mathbf{w}_h(\mathbf{a})|^2$. The numerical algorithm used in our computations is then as follows:

- Step 1. Specify a triangulation $\mathcal{T}_h^\epsilon$, the initial values $\mathbf{u}_h^0$, a constant $TOL > 0$, and set $n = 0$;
- Step 2. Solve Eq. (4.9) to obtain $\mathbf{w}_h$;
- Step 3. Compute $\mathbf{u}_h^{n+1} = \mathbf{u}_h^n + (t_{n+1} - t_n)\mathbf{w}_h$ and let $n = n + 1$;
- Step 4. If $\|\mathbf{w}_h\| < TOL$, stop; otherwise, go to Step 2.[f]

In Step 3, we choose the time step size $\delta t = t_{n+1} - t_n$ adaptively in the following manner. For each n, we compute $\mathbf{u}_h^{n+1}$ using the same value of δt as in the last step. We accept $\mathbf{u}_h^{n+1}$ if $I_h(\mathbf{u}_h^{n+1}) < I_h(\mathbf{u}_h^n)$ and $\det \nabla \mathbf{u}_h^{n+1}|_K > 0$ in each element. Otherwise, we decrease the time step by a pre-defined factor $\alpha \in (0, 1)$, i.e. we set $\delta t = \alpha \delta t$. This process is done iteratively until $\mathbf{u}_h^{n+1}$ is accepted. Based in numerical experiments, we work with $\alpha = 0.1$ and $t_1 - t_0 = 0.02$. In most time steps, no reductions of the form $\delta t = \alpha \delta t$ are necessary. To avoid the time step becoming smaller and smaller, we reset $\delta t = \delta t/\alpha$ every certain number M of steps. In our computations, we set $M = 100$. With this choice of parameters, the program runs fast in the beginning and finds the minimizers, up to a certain error, after a few thousands of steps.

[f] A better stop criteria would be $\|\mathbf{w}_h\| < TOL\|\mathbf{u}_h\|$, as suggested by the anonymous referee.

5. Numerical Experiments and Results

In our experiments we consider a two-dimensional body, occupying the unit disc in the plane as its reference configuration, with stored-energy function

$$W(\mathbf{F}) = 2|\mathbf{F}|^{\frac{3}{2}}/3 + (\det\mathbf{F} - 1)^2/2 + (\det\mathbf{F})^{-1}, \tag{5.1}$$

(it corresponds to $f(s) = (s-1)^2/2 + 1/s$, $p = \frac{3}{2}$ and $\mu = 1$ in (2.3)). We consider radial displacement boundary conditions of the form $\mathbf{u}(\mathbf{x}) = \lambda\mathbf{x}$ for $|\mathbf{x}| = 1$, with λ varying from 1.1 to 2.5. The initial radius ϵ of the microcavity was given various values from 0.005 to 0.05. The initial deformation specified was $\mathbf{u}(\mathbf{x})|_{t=0} = \lambda\mathbf{x}$.

The above choice of domain geometry and of boundary conditions was made for simplicity and for comparison with previous results. Our method can be applied also to more general geometries and boundary conditions.

5.1. *Validation and efficiency of the algorithm*

In this subsection we consider the simple example of a body with a single cavity, located at the centre.

Fig. 10 shows the initial and deformed configurations when $\epsilon = 0.01$ and $\lambda = 1.8$. The original cavity has increased about 100 times its size, which corresponds clearly to a cavitation singularity. Various initial conditions were considered, including some that are not radially symmetric, as those in Ref. 29 (e.g. $R_0(r) = \lambda r$, $\Theta_0(\theta) = \theta + 4r(1-r)$, where (R_0, Θ_0) and (r, θ) denote the polar coordinates of $\mathbf{u}_0$ and $\mathbf{x}$, respectively). The computations using these different initial conditions produced always almost the same deformed configuration. These results support the long-standing conjecture that for this choice of domain and boundary conditions the minimizer is radially symmetric (see Ref. 40, 41).

Fig. 11 shows the diminishment of the discrete energy I_h^ϵ and of the residual $\|\mathbf{w}_h\|$ with respect to the artificial time t. We observe that the energy decreases very fast and almost attains the minimal energy at $t = 7$ (the minimal time step observed in this experiment is 0.002). The residual $\|\mathbf{w}_h\|$ decreases exponentially.

Fig. 10. Reference and deformed configurations for $\epsilon = 0.01$, $\lambda = 1.8$.

Fig. 11. The discrete energy I_h^ϵ and $\|\mathbf{w}_h\|$ with respect to the artificial time t.

.

In order to validate and to study the efficiency of our numerical method, we compare our solutions to the two-dimensional minimization problem against the minimizers of the elastic energy among radially symmetric deformations. Even though the latter are not known explicitly (in the case of compressible elasticity, when

$W(F)$ is given by (2.3)), they can be computed numerically with very high precision, making the validation possible. Indeed, by writing $\mathbf{u}(\mathbf{x}) = u(r)\frac{\mathbf{x}}{r}$, with $r = |\mathbf{x}|$, the original problem (2.9) reduces to

$$\min_{u \in W^{1,p}(\epsilon,1);\, u(1)=\lambda} 2\pi \int_{\epsilon}^{1} \Phi(r, u, u') r dr, \tag{5.2}$$

where $\Phi(r, u, u') = \frac{\mu}{p}\left((u')^2 + \left(\frac{u}{r}\right)^2\right)^{\frac{p}{2}} + f(\frac{uu'}{r})$, which can be computed using very fine meshes (cf. Ref. 21). Denoting its numerical solution by $\tilde{u}_h(r)$, we can define the numerical error for the original problem as

$$err = \left\|\mathbf{u}_h - \tilde{u}_h(r)\frac{\mathbf{x}}{r}\right\|_{0,\Omega_\epsilon},$$

that is, the L^2 distance between $\mathbf{u}_h$ and $\tilde{u}_h(r)\frac{\mathbf{x}}{r}$.

Fig. 12 shows, for various ϵ, the convergence behavior of the computational error with respect to the number N_s of degrees of freedom, which represents the number of sides in the triangulation. For the comparison, we set $\lambda = 1.8$ (value at some distance of the critical displacement for cavitation, as observed in our computations) and considered the three different cases $\epsilon = 0.02, 0.01, 0.005$. For each case, solutions were computed using various triangulations, with respective values of N_s given by $190, 740, 2920, 11600$. For the meshes with the same N_s and different ϵ, the two mesh parameters N and δ, defined in Sections 3.2 and Section 3.3, remained invariant. Fig. 12 suggests two conclusions. First, the convergence order of the computational error is N_s^{-1} for all cases. Second, the convergence behavior for the nonconforming finite element method is not noticeably affected by changes in ϵ, confirming our analysis of Section 3.3.

Fig. 12. Error vs. degrees of freedom under various ϵ ($\lambda = 1.8$).

5.2. *Concordance with previous analyses and experiments*

In this subsection we present our results on the dependence of the cavity radius in the deformed configuration with respect to the displacement parameter λ. We show, in particular, the existence of a limiting profile for this relation as $\epsilon \to 0$, as well as the existence of a critical displacement for cavitation, in agreement with the analyses of Ball,[4] Sivaloganathan,[35] Horgan and Abeyaratne[19] and the experimental and theoretical study of Gent and Lindley[13].

Fig. 13 shows the relation between λ and the cavity radius, for the problem considered in the previous subsection (that of a ball with an ϵ microcavity at the origin, subjected to a radial stretch λ at the outer surface), for different values of ϵ. The cavity radius changes dramatically for values of λ between 1.4 and 1.5. This corresponds to the critical load for the opening of a cavity in the limit as $\epsilon \to 0$. For further results on the computation of the critical displacement and the generation

of the approximate bifurcation diagram, we refer to the novel numerical method of Negrón-Marrero and Sivaloganathan[30].

Fig. 13. Cavity radius vs. displacement λ at the boundary, for different values of ϵ.

Fig. 14 shows the tangential strain in the body for different values of λ. It verifies that in order to reduce the global energy, a minimizer will experience an enormous tangential strain. As discussed in Section 3.5, even though the tangential strain is large in the inner cavity, as $\epsilon \to 0$ the Jacobian determinants remain bounded and converge to the minimizer of f.

Fig. 14. Tangential strain vs. radius r under increasing λ.

Finally, an experiment of loading and subsequent unloading of the elastic body with a cavity at the centre was conducted in order to determine if hysteresis cycles were present. As Fig. 15 shows, no hysteresis was observed. This is relevant for a better understanding of the energy landscape associated to cavitation.

Fig. 15.

5.3. *New observations*

Using the numerical method presented in this paper, we were able to compute for the first time minimizers of the energy in a domain containing an off-centre cavity, as well as in a domain containing multiple cavities. Some of the computational results are presented in this subsection.

For the case of a domain with an off-centre cavity, Fig. 16 shows the deformed body for various choices of the location of the cavity in the reference configuration. We observe that the shape of the cavity is not greatly affected by changes in the location of the precursor microcavity. However, the size of the cavity becomes smaller as its initial location is displaced farther off the centre. The computed total energies for the different cases are 14.8495,15.1178,15.7653 and 16.0921. In particular, the energy becomes slightly larger as the cavity moves farther from the centre. This suggests that the optimal position for a single hole is at the origin (confirming the analysis of Ref. 37).

Fig. 16. Deformed configurations for various choices of the cavity position $\mathbf{a}$, with $\lambda = 2$ and $\epsilon = 0.01$.

We finally computed some examples with two precursor microcavities. The deformed configurations are shown in Fig. 17, Fig. 18 and Fig. 19. The results show

that when cavitation is energy favourable the body can be led to an unsustainable state of tension at the ligament between adjacent microcavities, which provides the body with a clear motivation to undergo fracture that is absent in the undeformed state. In turn, this shows that the models for cavitation in nonlinear elasticity may prove relevant for a better understanding of the mechanism of ductile fracture in metals by void coalescence (see, e.g., Petrinic et al.[34], Goods and Brown[14]).

Fig. 17. Initial and deformed configurations with two pre-existing cavities at (0,0) and at (0.3,0).

Fig. 18. Initial and deformed configurations with two pre-existing cavities at (0,0) and at (0.5,0).

Fig. 19. Initial and deformed configurations with two pre-existing cavities at (0.5,0) and at (-0.5,0).

Acknowlegement

The authors are grateful to Christoph Ortner and John M. Ball for their valuable discussions and suggestions, as well as to the anonymous referee whose comments have served to greatly improve various parts of the paper. The work was partly done during the first author's stay at the Mathematical Institute of the University of Oxford, visit supported financially by State Scholarship Fund of China. The first author would also like to thank the support of The State Key Laboratory of Scientific and Engineering Computing of China.

References

1. I. Babuska and A. K. Aziz, On the angle condition in the finite element method, *SIAM J. Numer. Anal.* **13** (1976) 214–226.
2. Y. Bai and Z.-P. Li, A truncation method for detecting singular minimizers involving the Lavrentiev phenomenon, *Math. Models Methods Appl. Sci.* **16** (2006) 847–867.
3. J. M. Ball, Convexity conditions and existence theorems in nonlinear elasticity, *Arch. Rational Mech. Anal.* **63** (1976/77) 337–403.
4. J. M. Ball, Discontinuous equilibrium solutions and cavitation in nonlinear elasticity, *Philos. Trans. R. Soc. A*, **306** (1982) 557–611.
5. J. M. Ball, Minimizers and the Euler-Lagrange equations, in *Trends and Applications of Pure Mathematics to Mechanics: Palaiseau, 1983* (Springer, Berlin, 1984), 1–4.
6. J. M. Ball and G. Knowles, A numerical method for detecting singular minimizers, *Numer. Math.* 51 (1987) 181–197.
7. J. M. Ball, Singularities and computation of minimizers for variational problems, in R. A. DeVore et al. (eds.), *Foundations of Computational Mathematics*, London Math. Soc. Lecture Note Ser. 284 (Cambridge University Press, Cambridge, 2001), 1–20.

8. J. M. Ball, Some open problems in elasticity, in *Geometry, Mechanics, and Dynamics* (Springer, New York, 2002), 3–59.
9. E. Burman and P. Hansbo, Stabilized Crouzeix-Raviart element for the Darcy-Stokes problem, *Numer. Methods Partial Differential Equations*, **21** (2005) 986–997.
10. S. Conti and C. De Lellis, Some remarks on the theory of elasticity for compressible Neohookean materials, *Ann. Scuola Norm. Super. Pisa Cl. Sci. (5)*, **2** (2003) 521–549.
11. M. Crouzeix and P.-A. Raviart, Conforming and nonconforming finite element methods for solving the stationary Stokes equations. I, *Rev. Française Automat. Informat. Recherche Opérationnelle Sér. Rouge*, **7** (1973) 33–75.
12. R. S. Falk, Nonconforming Finite Element Methods for the Equations of Linear Elasticity, *Math. Comp.* **57** (1991) 529–550.
13. A. N. Gent and P. B. Lindley, Internal rupture of bonded rubber cylinders in tension, *Proc. Roy. Soc. London Ser. A*, **249** (1958) 195–205.
14. S. H. Goods and L. M. Brown, The nucleation of cavities by plastic deformation, *Acta Metall.* **27** (1979) 1–15.
15. D. Henao, Cavitation, invertibility, and convergence of regularized minimizers in nonlinear elasticity, *J. Elast.* **94** (2009) 55–68.
16. D. Henao and C. Mora-Corral, Invertibility and weak continuity of the determinant for the modelling of cavitation and fracture in nonlinear elasticity, *Arch. Rational Mech. Anal.* **197** (2010) 619–655.
17. D. Henao and C. Mora-Corral, Fracture surfaces and the regularity of inverses for BV deformations, `http://www.maths.ox.ac.uk/groups/oxpde/technical-report-series`, preprint OxPDE-09/12.
18. D. Henao and C. Mora-Corral, Lusin's condition and the distributional determinant for Sobolev deformations with finite energy, `http://www.ann.jussieu.fr/publications/2009.php3`, preprint R09062.
19. C. O. Horgan and R. Abeyaratne, A bifurcation problem for a compressible nonlinearly elastic medium: growth of a micro-void, *J. Elast.* **16** (1986) 189–200.
20. C. O. Horgan and D. A. Polignone, Cavitation in nonlinearly elastic solids: a review, *Appl. Mech. Rev.* **48** (1995) 471–485.
21. G. Knowles, Finite element approximation to singular minimizers, and applications to cavitation in nonlinear elasticity, in *Differential Equations and Mathematical Physics*, Lecture Notes in Math. 1285 (Springer, Berlin, 1987), 236–247.

22. A. Lavrentiev, Sur quelques problemes du calcul des variations, *Ann. Mat. Pura Appl.* **41** (1926) 107–124.
23. Z.-P. Li, Element removal method for singular minimizers in varational problems involving Lavrentiev phenomenon, *Proc. Roy. Soc. London Ser. A*, **539** (1992) 131–137.
24. Y. Lian and Z. P. Li, A dual-parametric finite element method for cavitation in nonlinear elasticity, submitted for publication, 2010.
25. Y. Lian and Z. P. Li, A numerical study on cavitations in nonlinear elasticity: defects and configurational forces, submitted for publication, 2010.
26. K. W. Morton and F. F. Mayers, *Numerical Solution of Partial Differential Equations* (Cambridge University Press, Cambridge, 1994).
27. S. Müller, Det = det. A remark on the distributional determinant, *C. R. Acad. Sci. Paris Série I*, **311** (1990) 13–17.
28. S. Müller and S. J. Spector, An existence theory for nonlinear elasticity that allows for cavitation, *Arch. Rational Mech. Anal.* **131** (1995) 1–66.
29. P. V. Negrón-Marrero and O. Betancourt, The numerical computation of singular minimizers in two-dimensional elasticity, *J. Comput. Phys.* **113** (1994) 291–303.
30. P. V. Negrón-Marrero and J. Sivaloganathan, The numerical computation of the critical boundary displacement for radial cavitation, *Math. Mech. Solids*, **14** (2009) 696–726.
31. J. W. Neuberger, *Sobolev Gradients and Differential Equations*, Lecture Notes in Math. 1670 (Springer, Berlin, 1997).
32. C. Ortner, Nonconforming finite-element discretization of convex variational problems, *IMA J. Numer. Anal*, published online, 2010, doi:10.1093/imanum/drq004.
33. D. A. Polignone and C. O. Horgan, Cavitation for incompressible anisotropic nonlinearly elastic spheres, *J. Elast.* **33** (1993) 27–65.
34. N. Petrinic, J. L. Curiel Sosa, C. R. Siviour and B. C. F. Elliott, Improved predictive modeeling of strain localisation and ductile fracture in Ti-6Al-4V alloy subjected to impact loading, *J. Phys. IV France*, **134** (2006) 147–155.
35. J. Sivaloganathan, Uniqueness of regular and singular equilibria for spherically symmetric problems of nonlinear elasticity, *Arch. Rational Mech. Anal.* **96** (1986) 97–136.
36. J. Sivaloganathan and S. J. Spector, On the existence of minimizers with prescribed singular points in nonlinear elasticity, *J. Elast.* **59** (2000) 83–113.
37. J. Sivaloganathan and S. J. Spector, On the optimal location of singularities arising in variational problems in nonlinear elasticity, *J. Elast.* **58** (2000) 191–224.
38. J. Sivaloganathan and S. J. Spector, On cavitation, configurational forces and implications for fracture in a nonlinearly elastic material, *J. Elast.* **67** (2002) 25–49.
39. J. Sivaloganathan, S. J. Spector and V. Tilakraj, The convergence of regularized minimizers for cavitation problems in nonlinear elasticity, *SIAM J. Appl. Math.* **66** (2006) 736–757.
40. J. Sivaloganathan and S. J. Spector, On the symmetry of energy minimizing deformations in nonlinear elasticity I: incompressible materials, *Arch. Rational Mech. Anal.* **196** (2010) 363–394.
41. J. Sivaloganathan and S. J. Spector, On the symmetry of energy minimizing deformations in nonlinear elasticity II: compressible materials, *Arch. Rational Mech. Anal.* **196** (2010) 395–431.